**REVIEW ARTICLE**

# Pion PDFs confronted by fixed-target charmonium production

Wen-Chen Chang[1*] , Chia-Yu Hsieh[1], Yu-Shiang Lian[2], Jen-Chieh Peng[2], Stephane Platchkov[3] and Takahiro Sawada[4]

**Abstract**

The pion, as the Goldstone boson of the strong interaction, is the lightest QCD bound state and responsible for the long-range nucleon-nucleon interaction inside the nucleus. Our knowledge on the pion partonic structure is limited by the existing Drell-Yan data which are primarily sensitive to the pion valence-quark distributions. The recent progress of global analysis of pion's parton distribution functions (PDFs) utilizing various experimental approaches are introduced. From comparisons between the pion-induced $J/\psi$ and $\psi(2S)$ production data with theoretical calculations using the CEM and NRQCD models, we show how these charmonium production data could provide useful constraints on the pion PDFs.

**Keywords**  Pion PDFs, Charmonium, CEM, NRQCD

## 1 Introduction

The pion, being the Goldstone boson of dynamical chiral symmetry breaking of the strong interaction, is also the lightest QCD bound state. Because of its light mass, the pion plays a dominant role in the long-range nucleon-nucleon interaction. Understanding the pion's internal structure is important to investigate the low-energy, nonperturbative aspects of QCD [1]. Even though the pion is theoretically simpler than the proton, its partonic structure is much less explored. As scattering off a pion target is not feasible, current knowledge on pion PDFs mostly relies on the pion-induced Drell-Yan data [2]. Through the Drell-Yan reaction, the valence-quark distributions at $x > 0.2$ can be determined while additional

measurements are required to constrain the sea and gluon densities.

While the prompt-photon production process $\pi N \to \gamma X$ [3] was used to constrain the gluon content of pions through the $Gq \to \gamma q$ subprocess, the experimental uncertainties are large. Production of heavy quarkonia, like $J/\psi$ and $\Upsilon(1S)$, with a pion beam has distinctive advantages: the cross sections are large and their decay can be readily detected via the dimuon decay channel. These datasets have been shown to be sensitive to both the quark and gluon distributions of the incident pion [4, 5]. The other interesting approach of accessing the pion PDFs from the Sullivan process [6] in leading neutron deep inelastic scattering (DIS) data has been considered with promising results [7, 8]. This method is subject to large systematic uncertainties due to the off-shell nature of virtual pion in the fluctuated Fock state, and further theoretical studies are required to clarify the uncertainties [9, 10].

In the fixed-target energy domain, where the transverse momentum of the charmonium $J/\psi$ and $\psi(2S)$ is less than its mass, the charmonium production is dominated by the quark-antiquark ($q\bar{q}$) and gluon-gluon fusion ($GG$) partonic processes. The shape of the longitudinal

*Correspondence:
Wen-Chen Chang
changwc@phys.sinica.edu.tw
[1] Institute of Physics, Academia Sinica, Taipei 11529, Taiwan
[2] Department of Physics, University of Illinois at Urbana-Champaign, Urbana 61801, USA
[3] IRFU, CEA, Université Paris-Saclay, Gif-sur-Yvette 91191, France
[4] Institute for Cosmic Ray Research, The University of Tokyo, Gifu 506-1205, Japan

Chang *et al. AAPPS Bulletin*     (2023) 33:15

Page 2 of 9

**Table 1** Pion PDFs and utilized data sets

| PDFs | DY ($x_F$, $p_T$) | Direct $\gamma$ | $J/\psi$ | LN | Ref. |
|------|------|------|------|------|------|
| OW | √ | | √ | | [14] |
| ABFKW | √ | √ | | | [15] |
| SMRS | √ | √ | | | [16] |
| GRV | √ | √ | | | [17] |
| GRS | √ | | | | [21] |
| JAM18 | √ | | | √ | [19] |
| BS | √ | | | | [22–24] |
| xFitter | √ | √ | | | [18] |
| JAM21 | √ | | | √ | [20] |

momentum $x_F$ cross section is sensitive to the quark and gluon parton distributions of colliding hadrons. Since the nucleon PDFs are known with good accuracy, the measurement of total as well as the differential $x_F$ distribution of charmonia with the pion beam provides, within the theoretical model uncertainties, valuable information about the pion quark and gluon partonic distributions.

In this article, we present our recent studies about the possibility to constrain pion gluon density from the existing fixed-target charmonium data [11–13]. We start with an introduction of various pion PDFs and their distinctive features in Section 2, followed by Section 3 describing the two theoretical frameworks, CEM and NRQCD, used for describing the charmonium production. Section 4 shows the comparison of data and theoretical predictions, from which the differentiation of the large-$x$ gluon strengths in

various pion PDFs can be observed. We conclude with a summary of the results and a few remarks.

## 2 Pion PDFs

Pion-induced Drell-Yan data have been included in all global analyses for the determination of the pion PDFs. However, Drell-Yan process is mainly sensitive to the valence-quark distribution. Without additional observables, the sea and gluon distributions can be only inferred through the momentum and valence-quark sum rules. Different approaches have been taken to access the gluon and sea quark distributions: (i) utilizing $J/\psi$ production data in OW [14]; (ii) utilizing the direct-photon production data in ABFKW [15], SMRS [16], GRV [17], and xFitter [18]; (iii) utilizing the leading neutron DIS (LN) in JAM [19]; (iv) utilizing the production cross sections at the region of large transverse momentum ($p_T$) sensitive to NLO $qG$ process in JAM [20].

In addition, some pion PDFs are constructed based on theoretical modeling. For example, GRS [21] utilized a constituent quark model to relate the gluon and antiquark density, and BS [22–24] assumed quantum statistical distributions for all parton species with a universal temperature. The soft-gluon threshold resummation correction is known to modify the extraction of valence-quark distribution toward $x = 1$ [25] and how this effect modifies the large-$x$ behavior of valence quarks in a global analysis is recently examined [26]. We summarize the data sets used for various global analyses of pion PDFs in Table 1.
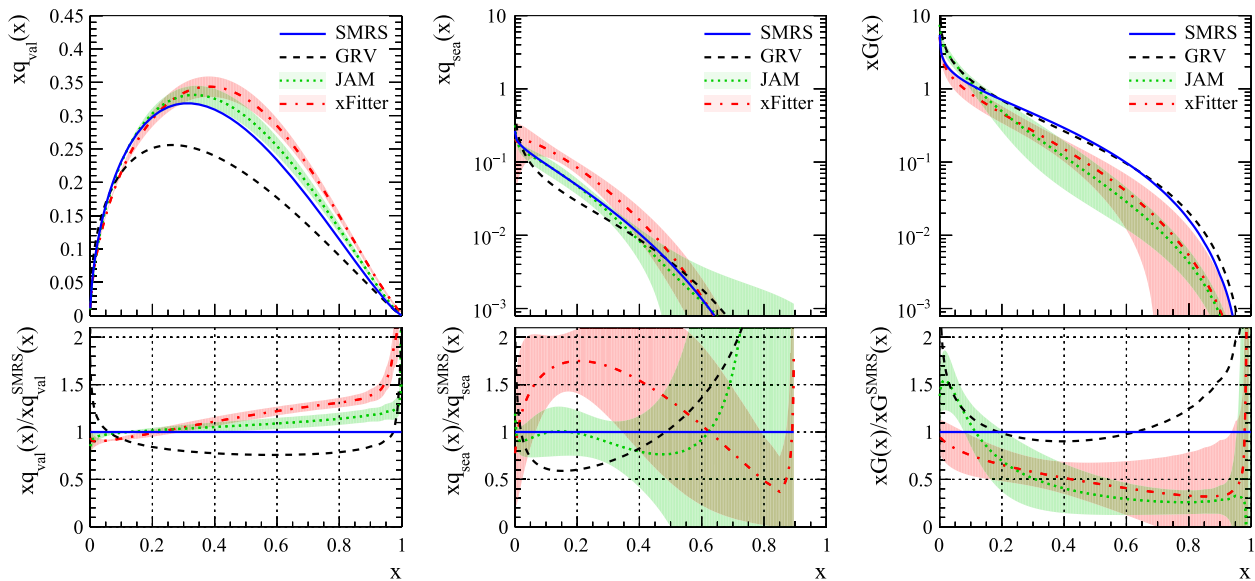


**Fig. 1** Momentum density distributions [$xf(x)$] of valence quarks, sea quarks and gluons of SMRS, GRV, xFitter, and JAM pion PDFs and their ratios to the SMRS PDFs, at the scale of $J/\psi$ mass ($Q^2$= 9.6 GeV$^2$) [13]. The quark flavor ($q$) is either u or d. The uncertainty bands associated with JAM and xFitter PDFs are shown

Chang *et al. AAPPS Bulletin*    (2023) 33:15

Page 3 of 9

**Table 2** Relationship of LDMEs and the associated orders of $\alpha_s$ to the scattering subprocesses for various charmonium states in the NRQCD framework of Ref. [39]. Here, $\Delta_8^H = \langle \mathcal{O}_8^H[^1S_0] \rangle + \frac{3}{m_c^2} \langle \mathcal{O}_8^H[^3P_0] \rangle + \frac{4}{5m_c^2} \langle \mathcal{O}_8^H[^3P_2] \rangle$

| $H$ | $q\bar{q}$ | $GG$ | $qG$ |
|---|---|---|---|
| $J/\psi, \psi(2S)$ | $\langle \mathcal{O}_8^H[^3S_1]\rangle(\alpha_s^2)$ | $\Delta_8^H(\alpha_s^2)\langle \mathcal{O}_1^H[^3S_1]\rangle(\alpha_s^3)$ | |
| $\chi_{c0}$ | $\langle \mathcal{O}_8^H[^3S_1]\rangle(\alpha_s^2)$ | $\langle \mathcal{O}_1^H[^3P_0]\rangle(\alpha_s^2)$ | |
| $\chi_{c1}$ | $\langle \mathcal{O}_8^H[^3S_1]\rangle(\alpha_s^2)$ | $\langle \mathcal{O}_1^H[^3P_1]\rangle(\alpha_s^3)$ | $\langle \mathcal{O}_1^H[^3P_1]\rangle(\alpha_s^3)$ |
| $\chi_{c2}$ | $\langle \mathcal{O}_8^H[^3S_1]\rangle(\alpha_s^2)$ | $\langle \mathcal{O}_1^H[^3P_2]\rangle(\alpha_s^2)$ | |

Figure 1 compares the valence, sea, and gluon momentum distributions of the SMRS, GRV, JAM, and xFitter pion PDFs at the scale of $J/\psi$ mass [13]. Their ratios to SMRS are shown in the bottom panel. Within the range of $x \sim$ 0.1–0.8, the valence-quark distributions of SMRS, JAM and xFitter are close to each other, whereas GRV is lower by

up to 20–30%. The sea distribution shows large variations between the four PDFs. The gluon distributions also show sizable differences; e.g., in the region of $x > 0.2$, the xFitter and JAM distributions are smaller in comparison with SMRS and GRV, by up to a factor of 2–3. As we will see in Section 4, these differences in the large-$x$ gluon distributions lead to quantitative difference in the data description of fixed-target charmonium data.

## 3 CEM and NRQCD models for charmonium production

Based on factorization, the theoretical description of charmonium production consists of the pQCD description of the production of $c\bar{c}$ pairs at the parton level [27–29], and their subsequent hadronization into the charmonium bound state [30, 31]. The latter nonperturbative part is challenging and has been modeled in theoretical approaches such as the color evaporation model (CEM) [32–34], the
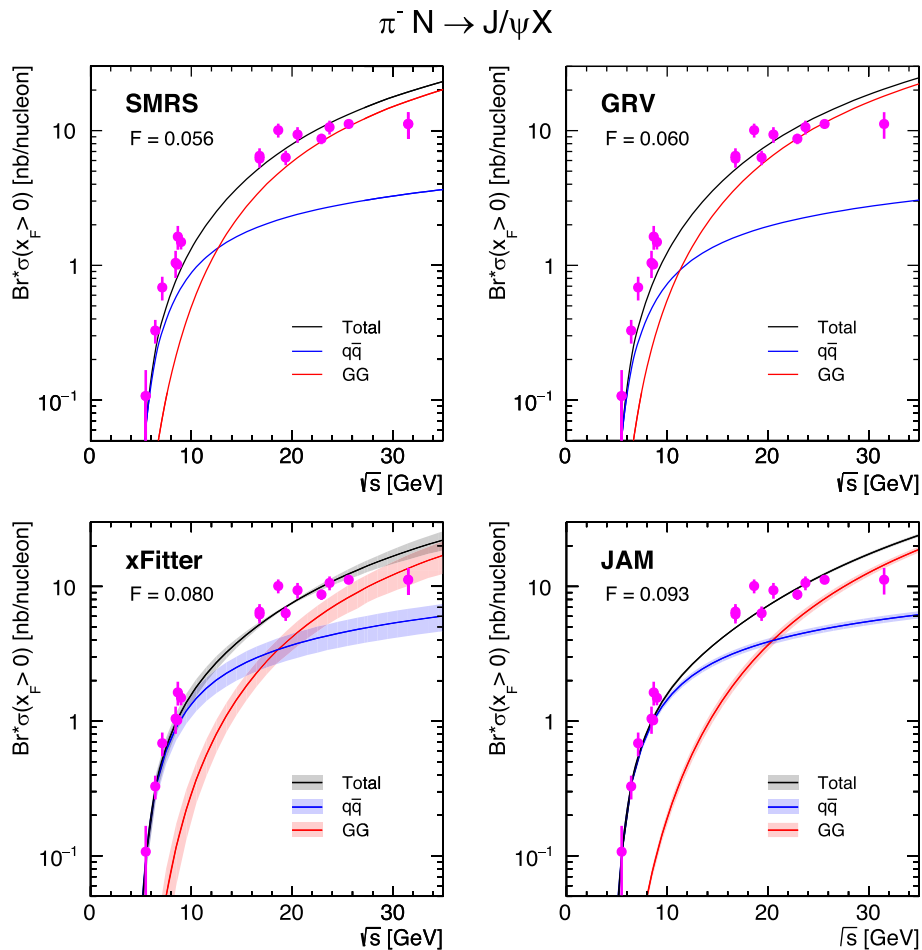


**Fig. 2** Comparison of $J/\psi$ dimuon decay branching ratio (Br) and $J/\psi$ production cross sections at $x_F > 0$ for the $\pi^-N$ reaction, calculated by the NLO CEM with four pion PDFs (SMRS, GRV, xFitter, and JAM) with the data (solid circles [45, 46]) [11]. The black, blue, and red curves represent the calculated total cross section and the $q\bar{q}$ and $GG$ contributions, respectively. The shaded bands on the xFitter and JAM calculations represent the uncertainties of the corresponding PDF sets

color-singlet model (CSM) [35–37], and the nonrelativistic QCD (NRQCD) [38, 39].

The CEM assumes a constant probability $F^H$, specific for each charmonium $H$, for the hadronization of $c\bar{c}$ pairs into the colorless hadron state. The differential cross section $d\sigma/dx_F$ for $J/\psi$ from the $\pi N$ collision is expressed as an integration of $c\bar{c}$ pair production with an invariant mass $M_{c\bar{c}}$ up to the $D\bar{D}$ threshold,

$$\frac{d\sigma^H}{dx_F} = F^H \sum_{i,j=q,\bar{q},G} \int_{2m_c}^{2m_D} dM_{c\bar{c}} \frac{2M_{c\bar{c}}}{s\sqrt{x_F^2 + 4M_{c\bar{c}}^2/s}}$$
$$\times f_i^\pi(x_1,\mu_F) f_j^N(x_2,\mu_F) \hat{\sigma}[ij \to c\bar{c}X](x_1 p_\pi, x_2 p_N, \mu_F, \mu_R),$$
(1)

$$x_F = 2p_L/\sqrt{s}, x_{1,2} = \frac{\sqrt{x_F^2 + 4M_{c\bar{c}}^2/s} \pm x_F}{2}$$
(2)

where $i$ and $j$ denote the interacting partons (gluons, quarks and antiquarks) and $m_c$, $m_D$, and $M_{c\bar{c}}$ are the masses of the charm quark, $D$ meson, and $c\bar{c}$ pair, respectively. The $f^\pi$ and $f^N$ are the corresponding pion and nucleon parton distribution functions, respectively,

evaluated at the corresponding Bjorken-$x$, $x_1$ and $x_2$, at the factorization scale $\mu_F$. The short-distance differential cross section of heavy-quark pair production $\hat{\sigma}[ij \to c\bar{c}X]$ is calculable as a perturbation series in the strong coupling $\alpha_s(\mu_R)$ evaluated at the renormalization scale $\mu_R$. The longitudinal momentum of the experimentally detected dilepton pair, equivalent to that of the $c\bar{c}$ pair, is denoted by $p_L$.

The $F^H$ factor is to be determined as the normalization parameter in the fit to the experimental measurements. The assumption of a common $F^H$ factor for different subprocesses greatly reduces the number of free parameters of the CEM. In spite of its well-known limitations [40], the CEM gives a good account of many features of fixed-target $J/\psi$ cross section data with proton beams, including their longitudinal momentum ($x_F$) distributions [41, 42] and the collider data at RHIC, Tevatron, and LHC [43, 44].

To examine a possible model dependence of observations, we carry out a similar study using NRQCD. The NRQCD factorization formula allows for a systematic expansion of inclusive quarkonium cross sections in
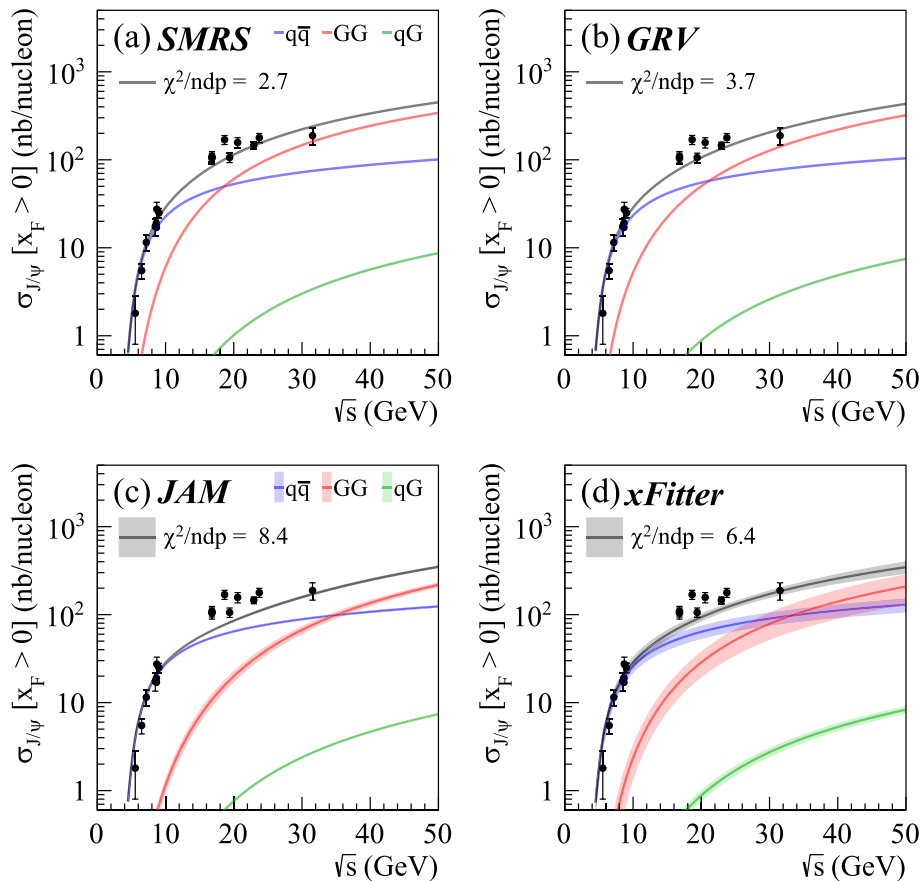


**Fig. 3** Same as Fig. 2 with the NRQCD calculations [12]

powers of the strong coupling constant $\alpha_s$ and the relative velocity $v$ of the heavy quarks. This expansion takes into account the short-distance production of color-singlet and color-octet $c\bar{c}$ precursor states with various spin ($S$), color ($n$), and angular momentum ($J$) quantum numbers. The long-distance matrix elements (LDMEs) are non-perturbative parameters that characterize the probability of a $c\bar{c}$ pair to evolve into a final quarkonium state. The LDMEs, assumed to be universal, are extracted from the experimental data. The differential cross section $d\sigma/dx_F$ for $J/\psi$ from the $\pi N$ collision is expressed as follows,

$$\frac{d\sigma^H}{dx_F} = \sum_{i,j=q,\bar{q},G} \int_0^1 dx_1 dx_2 \delta(x_F - x_1 + x_2)$$
$$\times f_i^h(x_1,\mu_F)f_j^N(x_2,\mu_F)\hat{\sigma}[ij \to H](x_1P_h, x_2P_N, \mu_F, \mu_R, m_c),$$
(3)

$$\hat{\sigma}[ij \to H] = \sum_n \hat{\sigma}[ij \to c\bar{c}[n]](x_1P_h, x_2P_N, \mu_F, \mu_R, m_c)\langle\mathcal{O}_n^H[^{2S+1}L_J]\rangle$$
(4)

where $\hat{\sigma}[ij \to c\bar{c}[n]]$ denotes the hard-QCD production cross section for $c\bar{c}$ pair of color state $n$ and $\langle\mathcal{O}_n^H[^{2S+1}L_J]\rangle$ is the corresponding LDME. Table 2 summarizes the relationships between the LDMEs and the scattering sub-processes for $J/\psi$, $\psi(2S)$, $\chi_{c0}$, $\chi_{c1}$, and $\chi_{c2}$, up to $\mathcal{O}(\alpha_s^3)$ in the NRQCD framework [39] adopted for computing $J/\psi$, $\psi(2S)$, and $\chi_{cJ}$ production via $GG$, $q\bar{q}$ and $qG$ subprocesses. The $J/\psi$ cross section is estimated taking into account the direct production of $J/\psi$ and the feed-down from hadronic decays of $\psi(2S)$ and radiative decays of three $\chi_{cJ}$ states.

## 4 Results and discussions
### 4.1 Integrated cross sections
We start with the comparison between the data of $\pi^- N \to J/\psi X$ cross sections integrated over $x_F > 0$ [45, 46] and the NLO CEM calculations with four pion PDFs, shown in Fig. 2. The evaluation of cross sections is done
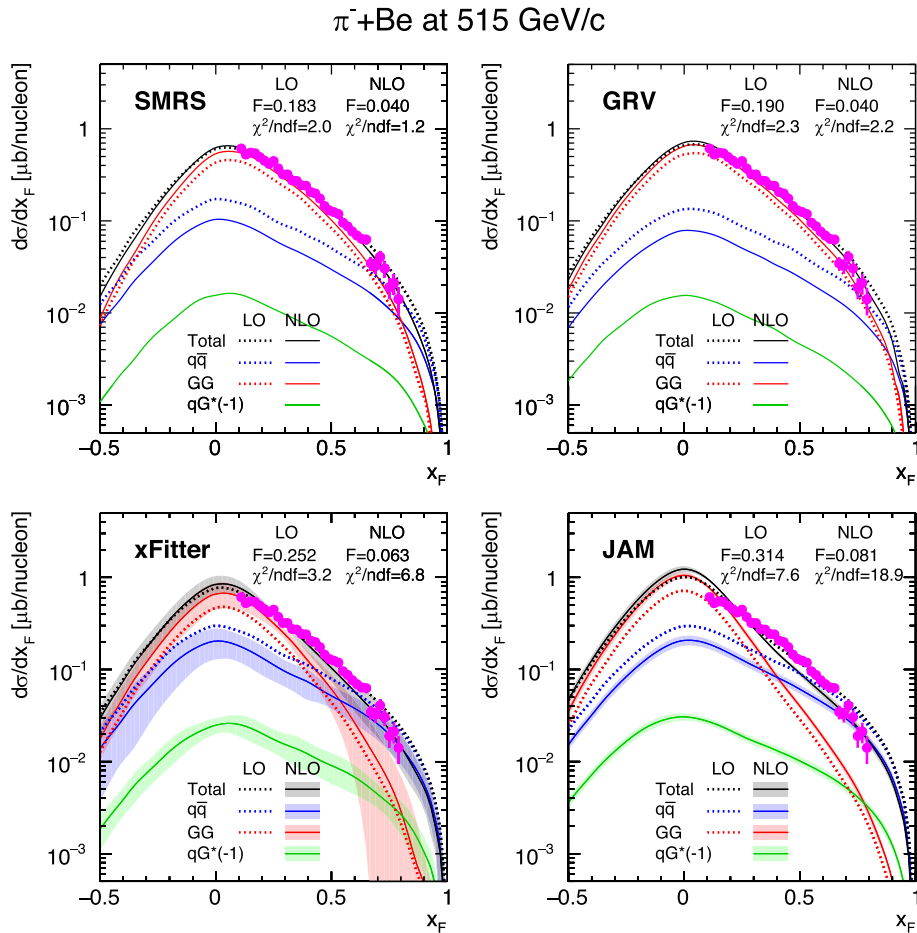


**Fig. 4** Comparison of the LO and NLO CEM results for the SMRS, GRV, xFitter, and JAM PDFs, with the $d\sigma/dx_F$ data [47] of $J/\psi$ production off the beryllium target with a 515-GeV/$c$ $\pi^-$ beam [11]. The total cross sections and $q\bar{q}$, $GG$, and $qG \times (-1)$ contributions are denoted as black, blue, red, and green lines, respectively. Solid and dotted lines are for the NLO and LO calculations, respectively. The shaded bands on the xFitter and JAM calculations come from the uncertainties of the corresponding PDF sets. The resulting $\chi^2$/ndf and $F$ factors are displayed

Chang *et al. AAPPS Bulletin*     (2023) 33:15

Page 6 of 9

with a charm quark mass $m_c = 1.5$ GeV/$c^2$ and renormalization and factorization scales of $\mu_R = m_c$ and $\mu_F = 2m_c$, respectively. The hadronization factors $F$ in the CEM model are assumed to be energy independent and determined by the best fit to the data for the central values of each pion PDF. The differences between them are visible through the $F$ factors, which vary from 0.05 to 0.09. Similar comparison made for the NRQCD calculations is shown in Fig. 3.

In the CEM study, the factor $F$ is determined by the best $\chi^2$ fit to each data set individually. In contrast, a global analysis of all data sets was performed to obtain some color-octet LDMEs as the fit parameters in the study with NRQCD. The quality of data description for each data set in NRQCD study is shown by $\chi^2$/ndp, where ndp denotes the number of degree of data points in a specific data set.

The total cross sections evaluated with the four PDFs exhibit quite similar $\sqrt{s}$ dependencies, and all agree reasonably with the data. The $q\bar{q}$ contribution dominates at low energies, whereas the $GG$ contribution becomes important with increasing $\sqrt{s}$. The relative fractions of $q\bar{q}$ and $GG$ contributions as a function of $\sqrt{s}$ vary for each pion PDFs, reflecting the differences between the corresponding parton distributions. For SMRS and GRV, the $GG$ contribution starts to dominate the cross section around $\sqrt{s} = 15$ GeV. For xFitter and JAM, the corresponding values are larger at $\sim \sqrt{s} = 20 - 30$ GeV because of their relatively reduced gluon strength in the valence region.

### 4.2 Differential $x_F$ cross sections

To investigate further the effect led by different pion PDFs, we compare the longitudinal $x_F$ distribution of the calculated pion-induced $J/\psi$ production cross section with a selection of fixed-target data from Fermilab and CERN experiments for pion-induced $J/\psi$ production as seen in Table II of Refs. [11, 13]. The beam momenta of the datasets cover the range of 39.5–515 GeV/$c$, corresponding to $\sqrt{s}$ values ranging from 8.6 to 31.1 GeV.

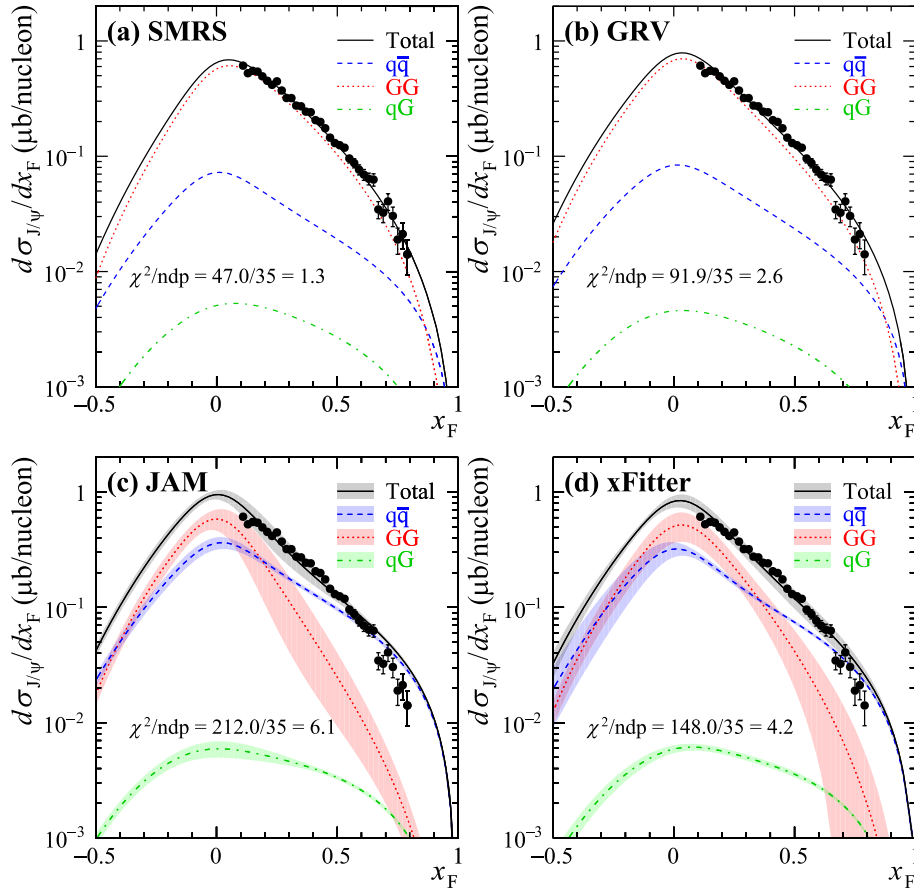The comparison of our LO and NLO CEM calculations to the E672/E706 data [47] with a 515 GeV/$c$ $\pi^-$



**Fig. 5** Same as Fig. 4 with the NRQCD calculations [13]

beam scattered off Be targets is shown in Fig. 4. Judging from the reduced $\chi^2$/ndf values, the NLO calculations with SMRS and GRV are in better agreement with the data than those with xFitter and JAM. The NLO calculation improves the description of the E672/E706 data only in the cases of SMRS and GRV. Figure 5 shows the same comparison with the NRQCD caluclations. It is also observed that SMRS and GRV are favored over JAM and xFitter in both comparisons with the CEM and NRQCD results.

The fraction of the $GG$ component is maximized around $x_F = 0$, corresponding to the gluon distribution $G_\pi(x)$ around $x \sim 0.1$–$0.2$. As a result of the rapid drop of the $G_\pi(x)$ toward $x = 1$, the $GG$ contribution quickly decreases at large $x_F$. In contrast, the $q\bar{q}$ contribution has a slower fall-off toward high $x_F$ because of a relatively strong pion valence antiquark density, in comparison with the gluon one, at large $x$. The ratio of $q\bar{q}$ to $GG$ shows a strong $x_F$ dependence, making the $x_F$-differential cross sections at high energies particularly sensitive to the shape of pion $G_\pi(x)$.

More information on the charmonium production mechanism can be obtained by comparing the production of the two charmonium states, $J/\psi$ and $\psi(2S)$. Figure 6 shows the comparison of the $\psi(2S)$ to $J/\psi$ ratios, $R_\psi(x_F)$, with the pion beam momentum of 252 GeV/$c$ [48] and the NRQCD calculations. An $x_F$-independent $R_\psi(x_F)$ is predicted by the CEM [49], since the fractions of $q\bar{q}$ and $GG$ components are identical for $J/\psi$ and $\psi(2S)$. In NRQCD, an $x_F$-dependent $R_\psi(x_F)$ is possible because different LDMEs are associated with the $q\bar{q}$ and $GG$ channels in evaluating the production of $J/\psi$ and $\psi(2S)$.

Figure 6 shows a strong $x_F$ dependence of $R_\psi$ and this suggests that the relative weights of the individual subprocesses $q\bar{q}$ and $GG$ components in $J/\psi$ and $\psi(2S)$ production are distinctly different. The pronounced rise in the $R_\psi(x_F)$ data at forward $x_F$, where the $q\bar{q}$ subprocess dominates the production, indicates that the $q\bar{q}$ subprocess is more important for the $\psi(2S)$ production than for the $J/\psi$ production. The comparison of this
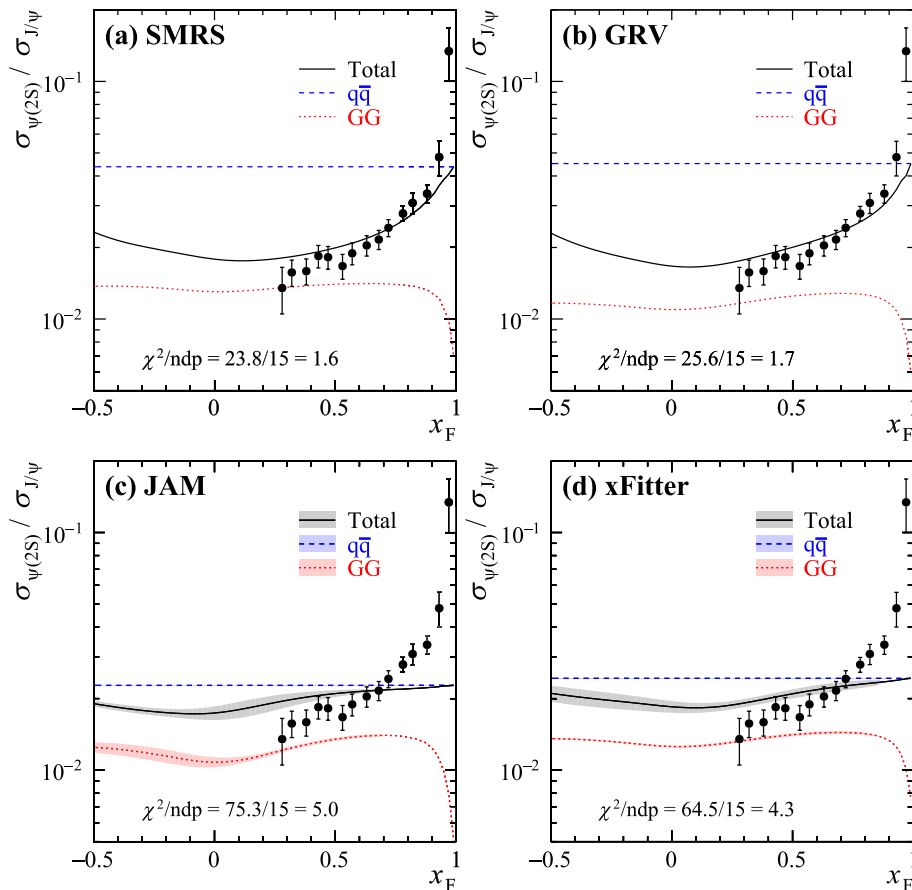


**Fig. 6** The $\psi(2S)$ to $J/\psi$ cross section ratios $R_\psi(x_F)$ for $J/\psi$ and $\psi(2S)$ production with a 252-GeV/$c$ $\pi^-$ beam [48]. The data are compared to the NRQCD calculations for the SMRS, GRV, xFitter, and JAM PDFs [13]. The ratios of total cross sections and individual $R_\psi^{q\bar{q}}(x_F)$ and $R_\psi^{GG}(x_F)$ contributions are denoted as solid black, dashed blue, and dotted red lines, respectively

Chang *et al. AAPPS Bulletin*    (2023) 33:15

Page 8 of 9

result remains to favor the calculations with SMRS and GRV, consistently with the observation with $J/\psi$ production data.

## 5 Summary

We examine the existing pion PDFs which exhibit pronounced differences, particularly in their gluon distributions. Using these PDFs as the input of CEM and NRQCD, the total and $x_F$ differential cross sections of pion-induced $J/\psi$ and $\psi(2S)$ production are calculated and compared to the fixed-target data.

We observe the importance of the gluon-gluon fusion process in charmonium production, especially at high (fixed-target) energies. Since the calculated shapes of $x_F$ distributions of $GG$ and $q\bar{q}$ contributions are directly related to the parton $x$ distributions of corresponding PDFs, a proper description of charmonium production data, especially for $x_F > 0.5$, imposes strong constraints on the relevant pion's parton densities. Among the four pion PDFs examined, both CEM and NRQCD calculations clearly favor SMRS and GRV PDFs whose gluon densities at $x > 0.1$ are stronger, compared with xFitter and JAM PDFs. The $GG$ contribution from the latter two pion PDFs drops too fast toward $x_F = 1$ to describe the data. While future theoretical developments are required to reduce the theoretical uncertainties in describing the charmonium production and thus improve the precision of the extracted PDFs, we emphasize the importance of including the pion-induced charmonium data in future pion PDF global analysis.

In the near future, new measurements of Drell-Yan as well as $J/\psi$ data in $\pi^-N$ reactions will be available from the CERN COMPASS [50] and AMBER [51] experiments. For the coming electron-ion collider projects in USA and China, the pion as well kaon structures are to be explored using the tagged DIS process [52–55]. To characterize the recoiled baryon system from the collisions with very small four-momentum transfer for the extraction of on-shell meson PDFs, a high-resolution zero-degree calorimeter is required. A collaboration of East Asian countries on developing this key detector for US EIC project was recently discussed [56].

### Authors' contributions
All authors equally contributed to the manuscript. Wen-Chen Chang is the lead author in organizing and writing the draft. All authors read, polished, and approved the final manuscript.

## Declarations

**Ethics approval and consent to participate**
N/A

**Consent for publication**
N/A

**Competing interests**
The authors declare that they have no competing interests.

### References

1. T. Horn, C.D. Roberts, The pion: an enigma within the Standard Model. J. Phys. G **43**(7), 073001 (2016). https://doi.org/10.1088/0954-3899/43/7/073001
2. W.C. Chang, D. Dutta, The pionic Drell-Yan process: a brief survey. Int. J. Mod. Phys. E **22**, 1330020 (2013). https://doi.org/10.1142/S0218301313300208
3. M. Bonesini et al., High transverse momentum prompt photon production by $\pi^-$ and $\pi^+$ on protons at 280 GeV/$c$. Z. Phys. C **37**, 535 (1988). https://doi.org/10.1007/BF01549712
4. M. Gluck, J.F. Owens, E. Reya, Gluon Contribution to Hadronic J/psi Production. Phys. Rev. D **17**, 2324 (1978). https://doi.org/10.1103/PhysRevD.17.2324
5. V.D. Barger, W.Y. Keung, R.J.N. Phillips, Hadroproduction of $\psi$ and $\Upsilon$. Z. Phys. C **6**, 169 (1980). https://doi.org/10.1007/BF01588844
6. J.D. Sullivan, One pion exchange and deep inelastic electron - nucleon scattering. Phys. Rev. D **5**, 1732–1737 (1972). https://doi.org/10.1103/PhysRevD.5.1732
7. V.A. Khoze, A.D. Martin, M.G. Ryskin, Information from leading neutrons at HERA. Eur. Phys. J. C **48**, 797–804 (2006). https://doi.org/10.1140/epjc/s10052-006-0015-7
8. J.R. McKenney, N. Sato, W. Melnitchouk, C.R. Ji, Pion structure function from leading neutron electroproduction and SU(2) flavor asymmetry. Phys. Rev. D **93**(5), 054011 (2016). https://doi.org/10.1103/PhysRevD.93.054011
9. S.X. Qin, C. Chen, C. Mezrag, C.D. Roberts, Off-shell persistence of composite pions and kaons. Phys. Rev. C **97**(1), 015203 (2018). https://doi.org/10.1103/PhysRevC.97.015203
10. R.J. Perry, A. Kızılersü, A.W. Thomas, Model dependence of the pion form factor extracted from pion electroproduction. Phys. Rev. C **100**(2), 025206 (2019). https://doi.org/10.1103/PhysRevC.100.025206
11. W.C. Chang, J.C. Peng, S. Platchkov, T. Sawada, Constraining gluon density of pions at large $x$ by pion-induced $J/\psi$ production. Phys. Rev. D **102**(5), 054024 (2020). https://doi.org/10.1103/PhysRevD.102.054024
12. C.Y. Hsieh, Y.S. Lian, W.C. Chang, J.C. Peng, S. Platchkov, T. Sawada, NRQCD analysis of charmonium production with pion and proton beams at fixed-target energies. Chin. J. Phys. **73**, 13–23 (2021). https://doi.org/10.1016/j.cjph.2021.06.001
13. W.C. Chang, J.C. Peng, S. Platchkov, T. Sawada, Fixed-target charmonium production and pion parton distributions. Phys. Rev. D **107**(5), 056008 (2023). https://doi.org/10.1103/PhysRevD.107.056008
14. J.F. Owens, $Q^2$-dependent parametrizations of pion parton distribution functions. Phys. Rev. D **30**, 943 (1984). https://doi.org/10.1103/PhysRevD.30.943
15. P. Aurenche, R. Baier, M. Fontannaz, M.N. Kienzle-Focacci, M. Werlen, The gluon content of the pion from high-$p_T$ direct photon production. Phys. Lett. B **233**, 517–521 (1989). https://doi.org/10.1016/0370-2693(89)91351-8

Chang *et al. AAPPS Bulletin* (2023) 33:15

Page 9 of 9

16. P.J. Sutton, A.D. Martin, R.G. Roberts, W.J. Stirling, Parton distributions for the pion extracted from Drell-Yan and prompt photon experiments. Phys. Rev. D **45**, 2349–2359 (1992). https://doi.org/10.1103/PhysRevD.45.2349

17. M. Gluck, E. Reya, A. Vogt, Pionic parton distributions. Z. Phys. C **53**, 651–656 (1992). https://doi.org/10.1007/BF01559743

18. I. Novikov et al., Parton Distribution Functions of the Charged Pion Within The xFitter Framework. Phys. Rev. D **102**(1), 014040 (2020). https://doi.org/10.1103/PhysRevD.102.014040

19. P.C. Barry, N. Sato, W. Melnitchouk, C.R. Ji, First Monte Carlo Global QCD Analysis of Pion Parton Distributions. Phys. Rev. Lett. **121**(15), 152001 (2018). https://doi.org/10.1103/PhysRevLett.121.152001

20. N.Y. Cao, P.C. Barry, N. Sato, W. Melnitchouk, Towards the three-dimensional parton structure of the pion: Integrating transverse momentum data into global QCD analysis. Phys. Rev. D **103**(11), 114014 (2021). https://doi.org/10.1103/PhysRevD.103.114014

21. M. Gluck, E. Reya, I. Schienbein, Pionic parton distributions revisited. Eur. Phys. J. C **10**, 313–317 (1999). https://doi.org/10.1007/s100529900124

22. C. Bourrely, J. Soffer, Statistical approach of pion parton distributions from Drell-Yan process. Nucl. Phys. A **981**, 118–129 (2019). https://doi.org/10.1016/j.nuclphysa.2018.07.003

23. C. Bourrely, F. Buccella, J.C. Peng, A new extraction of pion parton distributions in the statistical model. Phys. Lett. B **813**, 136021 (2021). https://doi.org/10.1016/j.physletb.2020.136021

24. C. Bourrely, W.C. Chang, J.C. Peng, Pion Partonic Distributions in the Statistical Model from Pion-induced Drell-Yan and J/Ψ Production Data. Phys. Rev. D **105**(7), 076018 (2022). https://doi.org/10.1103/PhysRevD.105.076018

25. M. Aicher, A. Schafer, W. Vogelsang, Soft-gluon resummation and the valence parton distribution function of the pion. Phys. Rev. Lett. **105**, 252003 (2010). https://doi.org/10.1103/PhysRevLett.105.252003

26. P.C. Barry, C.R. Ji, N. Sato, W. Melnitchouk, Global QCD Analysis of Pion Parton Distributions with Threshold Resummation. Phys. Rev. Lett. **127**(23), 232001 (2021). https://doi.org/10.1103/PhysRevLett.127.232001

27. P. Nason, S. Dawson, R.K. Ellis, The total cross section for the production of heavy quarks in hadronic collisions. Nucl. Phys. B **303**, 607–633 (1988). https://doi.org/10.1016/0550-3213(88)90422-1

28. P. Nason, S. Dawson, R.K. Ellis, The One Particle Inclusive Differential Cross-Section for Heavy Quark Production in Hadronic Collisions. Nucl. Phys. B **327**, 49–92 (1989). https://doi.org/10.1016/0550-3213(89)90286-1

29. M.L. Mangano, P. Nason, G. Ridolfi, Fixed target hadroproduction of heavy quarks. Nucl. Phys. B **405**, 507–535 (1993). https://doi.org/10.1016/0550-3213(93)90557-6

30. N. Brambilla et al., Heavy Quarkonium: Progress, Puzzles, and Opportunities. Eur. Phys. J. C **71**, 1534 (2011). https://doi.org/10.1140/epjc/s10052-010-1534-9

31. J.P. Lansberg, New Observables in Inclusive Production of Quarkonia. Phys. Rept. **889**, 1–106 (2020). https://doi.org/10.1016/j.physrep.2020.08.007

32. M.B. Einhorn, S.D. Ellis, Hadronic Production of the New Resonances: Probing Gluon Distributions. Phys. Rev. D **12**, 2007 (1975). https://doi.org/10.1103/PhysRevD.12.2007

33. H. Fritzsch, Producing Heavy Quark Flavors in Hadronic Collisions: A Test of Quantum Chromodynamics. Phys. Lett. B **67**, 217–221 (1977). https://doi.org/10.1016/0370-2693(77)90108-3

34. F. Halzen, Cvc for Gluons and Hadroproduction of Quark Flavors. Phys. Lett. B **69**, 105–108 (1977). https://doi.org/10.1016/0370-2693(77)90144-7

35. C.H. Chang, Hadronic Production of J/ψ Associated With a Gluon. Nucl. Phys. B **172**, 425–434 (1980). https://doi.org/10.1016/0550-3213(80)90175-3

36. E.L. Berger, D.L. Jones, Inelastic Photoproduction of J/psi and Upsilon by Gluons. Phys. Rev. D **23**, 1521–1530 (1981). https://doi.org/10.1103/PhysRevD.23.1521

37. R. Baier, R. Ruckl, Hadronic Collisions: A Quarkonium Factory. Z. Phys. C **19**, 251 (1983). https://doi.org/10.1007/BF01572254

38. G.T. Bodwin, E. Braaten, G.P. Lepage, Rigorous QCD analysis of inclusive annihilation and production of heavy quarkonium. Phys. Rev. D **51**, 1125–1171 (1995). https://doi.org/10.1103/PhysRevD.55.5853

39. M. Beneke, I.Z. Rothstein, Hadroproduction of quarkonia in fixed target experiments. Phys. Rev. D **54**, 2005 (1996). https://doi.org/10.1103/PhysRevD.54.2005

40. G.T. Bodwin, E. Braaten, J. Lee, Comparison of the color-evaporation model and the NRQCD factorization approach in charmonium production. Phys. Rev. D **72**, 014004 (2005). https://doi.org/10.1103/PhysRevD.72.014004

41. R. Gavai, D. Kharzeev, H. Satz, G.A. Schuler, K. Sridhar, R. Vogt, Quarkonium production in hadronic collisions. Int. J. Mod. Phys. A **10**, 3043–3070 (1995). https://doi.org/10.1142/S0217751X95001443

42. G.A. Schuler, R. Vogt, Systematics of quarkonium production. Phys. Lett. B **387**, 181–186 (1996). https://doi.org/10.1016/0370-2693(96)00999-9

43. R.E. Nelson, R. Vogt, A.D. Frawley, Narrowing the uncertainty on the total charm cross section and its effect on the J/ψ cross section. Phys. Rev. C **87**(1), 014,908 (2013). https://doi.org/10.1103/PhysRevC.87.014908

44. J.P. Lansberg, H.S. Shao, N. Yamanaka, Y.J. Zhang, C. Noûs, Complete NLO QCD study of single- and double-quarkonium hadroproduction in the colour-evaporation model at the Tevatron and the LHC. Phys. Lett. B **807**, 135559 (2020). https://doi.org/10.1016/j.physletb.2020.135559

45. G.A. Schuler, Quarkonium production and decays. Ph.D. thesis, Hamburg U. (1994)

46. Y. Alexandrov et al., Inclusive J/ψ and ψ′ production in π⁻-nucleus interactions at $\sqrt{s} \simeq$ 26 GeV. Nucl. Phys. B **557**, 3–21 (1999). https://doi.org/10.1016/S0550-3213(99)00412-5

47. A. Gribushin et al., Production of J/ψ and ψ(2S) mesons in π⁻-Be collisions at 515 GeV/c. Phys. Rev. D **53**, 4723–4733 (1996). https://doi.org/10.1103/PhysRevD.53.4723

48. J.G. Heinrich et al., Higher-twist effects in the reaction $\pi N \rightarrow \mu^+ \mu^- X$ at 253 GeV/c. Phys. Rev. D **44**, 1909–1932 (1991). https://doi.org/10.1103/PhysRevD.44.1909

49. I. Abt et al., A Measurement of the ψ′ to J/ψ production ratio in 920 GeV proton-nucleus interactions. Eur. Phys. J. C **49**, 545–558 (2007). https://doi.org/10.1140/epjc/s10052-006-0139-9

50. M. Aghasyan, et al., First measurement of transverse-spin-dependent azimuthal asymmetries in the Drell-Yan process. Phys. Rev. Lett. **119**(11), 112,002 (2017). https://doi.org/10.1103/PhysRevLett.119.112002

51. B. Adams, et al., Letter of Intent: A New QCD facility at the M2 beam line of the CERN SPS (COMPASS++/AMBER). (2018)

52. A.C. Aguilar et al., Pion and Kaon Structure at the Electron-Ion Collider. Eur. Phys. J. A **55**(10), 190 (2019). https://doi.org/10.1140/epja/i2019-12885-0

53. J. Arrington et al., Revealing the structure of light pseudoscalar mesons at the electron–ion collider. J. Phys. G **48**(7), 075106 (2021). https://doi.org/10.1088/1361-6471/abf5c3

54. G. Xie, C. Han, R. Wang, X. Chen, Tackling the kaon structure function at EicC *. Chin. Phys. C **46**(6), 064107 (2022). https://doi.org/10.1088/1674-1137/ac5b0e

55. J.M.M. Chávez, V. Bertone, F. De Soto Borrero, M. Defurne, C. Mezrag, H. Moutarde, J. Rodríguez-Quintero, J. Segovia, Accessing the Pion 3D Structure at US and China Electron-Ion Colliders. Phys. Rev. Lett. **128**(20), 202501 (2022). https://doi.org/10.1103/PhysRevLett.128.202501

56. NCU workshop on EIC physics and detectors (2022). https://indico.phys.sinica.edu.tw/event/67/. Accessed 5 July 2023.

## Publisher's Note